Published in final edited form as:
J Magn Reson. 2009 September ; 200(1): 95–100. doi:10.1016/j.jmr.2009.06.009.

High-resolution solid-state NMR structure of Alanyl-Prolyl-Glycine

Alexander B. Barnes[a], **Loren B. Andreas**[a,b], **Matthias Huber**[a,c], **Ramesh Ramachandran**[a,d], **Patrick C.A. van der Wel**[a,e], **Mikhail Veshtort**[a], **Robert G. Griffin**[a], and **Manish A. Mehta**[b,*]

[a]Department of Chemistry and Francis Bitter Magnet Laboratory, Massachusetts, Institute of Technology, Cambridge, MA 02139, USA [b]Department of Chemistry, Oberlin College, 119 Woodland Street, Oberlin, OH 44074, USA [c]ETH Zurich, Physical Chemistry, Wolfgang-Pauli-Strasse 10, 8093 Zurich, Switzerland [d]Indian Institute of Science Education Research (IISER), Mohali, Chandigarh, India [e]University of Pittsburgh, Department of Structural Biology, Pittsburgh, PA 15260, USA

Abstract

We present a *de novo* high-resolution structure of the peptide Alanyl-Prolyl-Glycine using a combination of sensitive solid-state NMR techniques that each yield precise structural constraints. High-quality ^{13}C–^{13}C distance constraints are extracted by fitting rotational resonance width (R^2W) experiments using Multimode Multipole Floquet Theory and experimental chemical shift anisotropy (CSA) orientations. In this strategy, a structure is first calculated using DANTE-REDOR and torsion angle measurements and the resulting relative CSA orientations are used as an input parameter in the ^{13}C–^{13}C distance calculations. Finally, a refined structure is calculated using all the constraints. We investigate the effect of different structural constraints on structure quality, as determined by comparison to the crystal structure and also self-consistency of the calculated structures. Inclusion of all or subsets of these constraints into CNS calculations resulted in high-quality structures (0.02 Å backbone RMSD using all 11 constraints).

Keywords

SSNMR; Structural determination

1. Introduction

Determining the high-resolution structures (backbone RMSD < 0.1 Å) of uniformly labeled polypeptides with solid-state NMR is often prohibitively difficult due to a lack of precision available with homonuclear broadbanded recoupling techniques such as RAD [1], DARR [2] and TSAR [3]. Although these experiments can define the secondary and tertiary structure and yield a clear global structure of the protein, the lack of high-precision measurements can leave detail of the active site and mechanisms that are of broader interest

*Corresponding author. Fax: +1 440 775 6682. Manish.Mehta@oberlin.edu (M.A. Mehta).

to the biological community still undefined. More precise techniques such as REDOR [4], RFDR [5], DRAWS [6], and local field correlations yield sub-angstrom precision, but are often limited to spin-pair labeled systems.

A previous study on the polypeptide, N-*f*-MLF-OH, demonstrated the use of FS-REDOR, and torsion angle constraints to determine a high-resolution *de novo* structure [7]. Since the publication of that structure, additional high-resolution techniques applicable to uniformly ^{13}C, ^{15}N labeled systems have been developed, such as rotational resonance width (R^2W) [8,9] and DANTE-REDOR [10]. DANTE-REDOR can yield high-quality restrictions on torsion angles, in addition to heteronuclear distance constraints. R^2W utilizes band-selective R^2 to recouple homonuclear spin pairs and can separate weaker dipolar oscillations (from long distance, structurally relevant spin pairs) from relaxation processes using a constant mixing time strategy and has been recently applied to measure distances in uniformly labeled proteins [11]. However, Ramachandran et al. [12] discussed the effect of the relative CSA orientation of the two spins in extracting accurate distances from R^2W experiments. To make R^2W a truly *de novo*, precise, and accurate technique for making homonuclear distance measurements, one must obtain the relative CSA orientation of the spin pair experimentally.

We demonstrate the utility of an iterative approach to structure determination of uniformly labeled polypeptides using various solid-state NMR methods. Namely, ψ torsion angle and ^{13}C–^{15}N distances from NCCN [13] and DANTE-REDOR measurements are first used to establish a structure from which approximate relative CSA orientations are available. Those orientations are then utilized into the fitting routines of R^2W profiles to also obtain precise and accurate ^{13}C–^{13}C distances. Finally all experimentally determined homonuclear, heteronuclear, and torsion angles constraints are used in a final energy minimization that yields a high-quality *de novo* structure. We further discuss the effect of each sub-group of structural constraints on the structural quality as judged by self-consistent backbone RMSD and comparison to the known crystal structure.

2. Results and discussion

Fig. 1 shows the 11 constraints determined for APG listed in Table 1. Comparison with the X-ray crystal structure indicates the level of accuracy achieved in each measurement. Two of the restrictions on ψ dihedral angles were determined with a local field NCCN experiment [13]. DANTE-REDOR was used to determine the glycine ψ angle, and four ^{13}C–^{15}N internuclear distances. The four carbon internuclear distances were extracted using R^2W.

2.1. CSA parameters for precise R^2W fitting

The CSA magnitude and relative orientation of the two spins being recoupled by R^2 has a profound impact on the spin dynamics [15] and accuracy of the distances extracted using R^2W [12]. For example Fig. 2b shows the distribution of distances resulting using different CSA orientations taken from an ensemble of structures generated from simulated annealing without experimental constraints. The range of motion displayed in unconstrained simulated annealing is large enough even in this small molecule to cause substantial deviation in the

final R^2 calculations, which demonstrates the importance of first calculating a lower resolution structure.

As a starting point in the R^2W fitting routine, an initial structure based on REDOR and torsion angle measurements was first calculated. The relative CSA orientation from this structure was then used as an input for the R^2W fitting routine, which is derived from a Multimode Multipole Floquet Theory (MMFT) treatment of the two spins [16]. The ^{13}C–^{13}C distances from these R^2W fits were then used together with the REDOR and torsion angle constraints to calculate a final structure. R^2W fits generated with relative CSA orientations found in the final structure yielded the same distance as those generated from the initial REDOR-torsion angle structure. Thus we found it unnecessary to perform further iterations in which the structure generated with initial R^2W distance constraints is used to refine these constraints.

The default values from SIMMOL were used for relative CSA – molecular orientations, the span and skew of carbonyl carbons were extracted from a 4 kHz CP-MAS spectrum according to Herzfeld and Berger [18], and aliphatic carbon span and skew values were taken from Ye et al. [19].

2.2. Carboxyl terminus

The carboxyl terminus is not well defined due to the absence of ^{13}C–^{13}C constraints to the Gly carboxyl carbon (see Fig. 1). This is predominantly due to intermolecular and dipolar truncation effects complicating any ^{13}C–^{13}C distance measurements between the Gly C′ and the Pro C^{α} and Pro C^{β}. The Pro C^{β} carbon to Gly C′ carbon intermolecular distance is 5.5 Å in the crystal structure, but there are three other intermolecular Pro C^{β} to Gly C′ separations that are less than 5.4 Å (see Fig. 3). The crystals consisted of 10% ^{13}C–labeled peptide diluted with natural abundance APG to reduce the number of intermolecular contacts, however there still appears to be enough coupling between intermolecular Pro C^{β}–Gly C′ pairs to substantially effect the R^2W profile and result in a fitting of the data to 4.7 Å rather than 5.5 Å seen in the crystal structure.

Furthermore, the one-bond Pro C′–Pro C^{α} dipolar coupling truncates the Pro C′–Gly C^{α} coupling which would also constrain the carboxyl terminus. Even though R^2W is a band-selective recoupling technique and thus usually does not suffer from dipolar truncation [20], the single bond coupling is an order of magnitude stronger than the coupling of interest and is also recoupled when the spinning frequency is set to the $N = 2$ recoupling condition for the Pro C′ to Gly C^{α} interaction; the stronger coupling dominates and insufficient polarization is transferred to the Gly C^{α}. We note that the dipolar truncation should not be as pronounced at higher magnetic fields where the resonances are more separated and the recoupling condition is thus more selective.

2.3. Constraints effect on structural quality

The standard annealing protocol in the program CNS [21,22] was used to generate 40 APG structures in order to generate an ensemble that shows both an average geometry and

demonstrates the degree of conformational variability allowed by the geometrical constraints.

In order to compare the usefulness of different structural constraints, a backbone RMSD among the 40 structures of each ensemble was calculated. This shows the level of precision attained by the different NMR experiments, indicating their ability to define overall conformation in this peptide. The results are summarized in Fig. 4 and show excellent agreement with the crystal structure. Since we were not able to perform a measurement that constrains the ψ_{Gly} angle, the Gly carboxyl group was omitted from the RMSD calculations. The final NMR structure and the crystal structure agree to within an RMSD of 0.09 Å.

3. Conclusions

Precise ^{13}C–^{13}C, ^{13}C–^{15}N, and ψ torsion angles were measured in a uniformly ^{13}C, ^{15}N labeled peptide using R^2W in a *de novo* manner, DANTE-REDOR and local field NCCN experiments. Using these sub-angstrom structural constraints we were able to determine a high-quality structure of APG. The 0.02 Å backbone RMSD structure was sufficient to observe the same conformational heterogeneity of the proline ring that is seen in the X-ray structure at 100 K. The ability to discriminate the two conformers by using structural constraints with sub-angstrom precision and CNS could be applied to address biological questions that require high-resolution structural detail. Furthermore, the short intramolecular contacts present in the tripeptide lattice studied here should not be present in larger proteins and should enable the extension of this *de novo* R^2W strategy to distances up to 8 Å.

Finally, the NCCN torsion and many of the internuclear distances that were experimentally determined with SSNMR are indicative of *trans*-proline. Although proline is almost always in the *trans*-isomer, the isomerization to the cis can play an important role in mitotic regulation [23], and we emphasize the strategies for structure determination presented here could be used to further investigate the biological function of proline isomerization.

4. Experimental methods

4.1. Sample preparation

Experiments were performed on a sample of uniformly ^{13}C and ^{15}N labeled Alanyl-Prolyl-Glycine (APG) that was diluted to 10% in the corresponding natural abundance tripeptide to attenuate intermolecular dipolar couplings. The tripeptide was synthesized by CS Bio (CA) with labeled amino acids from Cambridge Isotopes (Andover, MA) and natural abundance material from BaChem (Switzerland). A 9:1 natural abundance to labeled APG mixture was dissolved in a minimal amount of water (solubility was approximately 45 mg/ml). The aqueous solution was placed in a desiccator next to a container of excess ethylene glycol. After a week, crystals were collected, crushed and packed into a rotor.

4.2. Assignments

To assign the ^{13}C resonances, a 2D ^{13}C–^{13}C SPC-5 [24] spectrum was recorded spinning at $\omega_r/2\pi$ = 7.5 kHz using TPPM decoupling [25]. γB_1 for ^{13}C was set to 37.5 kHz required by the recoupling condition. The mixing time was 1.07 ms corresponding to 16 rotor cycles,

during which time a 120 kHz continuous wave γB_1 field was applied on the proton channel for decoupling. In the indirect dimension, 256 time points were recorded using 16 scans for each t_1 point. The overall measurement time was 7 h. The direct and indirect dimensions were linearly predicted forward to 1024 points, zero-filled to 2048 points and Fourier transformed using NMRPIPE [26].

4.3. NCCN local field correlations

The torsion angles, ψ_{Ala} and ψ_{Pro} were determined with the double-quantum heteronuclear local field experiment previously described [13]. SPC-5 [24] was used to create the ^{13}C–^{13}C double-quantum coherence. The homonuclear mixing time was 800 μs, corresponding to eight rotor periods and the ^{13}C carrier was set precisely between the two resonances targeted for recoupling. γB_1 equal to 50 kHz was used for both ^{13}C and ^{15}N during homonuclear mixing and the REDOR [4] dephasing pulses. The spinning frequency was 10 and 110 kHz continuous wave γB_1 decoupling field on protons was applied during SPC-5 mixing and REDOR periods; 136 kHz TPPM [25] decoupling was used during the acquisition period. About 512 scans were taken per dephasing time, and a 3 s recycle delay was used between scans. Each dephasing point was normalized to the intensity of the corresponding resonances absent of REDOR pulses during the dephasing period. The resonances were integrated and the intensities fit (see Fig. 8) to extract the torsion angle with SPINEVOLUTION [27].

4.4. Rotational resonance width

NMR spectra were recorded on a 360 MHz Spectrometer (courtesy of Dr. D.J. Ruben) with a commercial Chemagnetics triple resonance MAS probe equipped with a 4.0 mm Chemagnetics spinning module. Spinning frequencies were regulated with a Bruker MAS controller.

The crosspeak volumes (see Fig. 7) were extracted by automated fitting to two-dimensional Gaussians using NMRPIPE [26]. All data points in each 2D-slice were normalized to the carbonyl intensities of reference experiments conducted at identical spinning frequencies with zero mixing time.

A Gaussian pulse of 250 μs duration was used, followed by a z-filter of 750 μs to select the carbonyl region of the spectrum. 32 t_1 points were recorded with an increment of 250 μs and 16 scans per point with a recycle delay of 3.1 s leading to a total experimental time of about 50 min per two-dimensional slice. A series of experiments were performed as a function of the sample spinning frequency under a constant mixing time of 30 ms (see Fig. 5).

4.5. DANTE-REDOR

DANTE-REDOR measurements were carried out on a custom assembled NMR spectrometer with a Discovery console (Tecmag; Houston, TX), 14.1 T magnet (Magnex; Oxford, England), and a 39-channel matrix shim system (Resonance Research, Inc.; Billerica, MA), operating at a proton frequency of 600.377 MHz (150.987 MHz for ^{13}C). A doubly tuned 4 mm magic angle spinning probe (Doty Scientific; Columbia, South Carolina) was employed.

The DANTE-REDOR pulse sequence is described in [10] and follows after DANTE-REDOR based work of Kaustov [28] and Schaefer [29]. This sequence adapts the orientation information available in a specifically labeled sample to a uniformly labeled system. By employing a DANTE pulse train as the selective pulse in FS-REDOR, the orientation information in REDOR sidebands is retained. Thus at the end of the REDOR evolution time, the ^{13}C spin-echo intensity is modulated only by dipolar couplings to the selected ^{15}N and the resulting REDOR curve can be fit to the analytical expression for an isolated spin pair. The effects of proton couplings are attenuated with Small Phase Incremental Alternation (SPINAL-64) decoupling [25]. The proton decoupling field was 100 kHz, the ^{15}N REDOR π-pulse width was 16 us and the DANTE π-pulse trains consisted of 33 2 μs rotor synchronized pulses.

Fourier transforms were applied with no apodization and zero filling to twice the acquisition time of 15.36 ms. Only zero order phase correction was used. Dephasing (S) and full-echo (S_0) peak areas were determined by integrating the center band and all observed sidebands. For distance determinations, the sum of all bands in the S and S_0 spectra were used. For extraction of orientation information, the dephasing of each individual band was compared.

Distances were determined by fitting the experimentally observed REDOR curve to the analytical expression, $\Delta S/S_0(\tau) = \lambda[1 - \langle\cos(\omega_{CN}\tau)\rangle]$. $\Delta S/S_0 = 1 - S/S_0$, where S and S_0 are the dipolar dephasing and reference intensities, respectively. The coupling ω_{CN} is a function of the dipolar coupling constant, b_{CN}, and $\langle\rangle$ indicates the powder average over a uniform distribution of crystallite orientations. The scaling factor λ accounts for ^{13}C spins without a neighboring ^{15}N spin, which is a result of imperfect labeling and dilution of the labeled compound in natural abundance material. In the DANTE-REDOR experiment, λ also accounts for imperfect inversion of the ^{15}N spin magnetization by the selective pulse and decay of coherence due to insufficient decoupling.

For each distance measurement, the weighted χ^2, χ^2_ν, was minimized to fit the data. $\chi^2_\nu \propto \sum_i w_i(S_{i,\mathrm{exp}} - S_{i,\mathrm{sim}})^2$. In this expression, w_i is the inverse uncertainty in each point squared (σ^{-2}). Since the noise in each data point is approximately constant, w_i was easily determined by propagation of error. In the minimization of χ^2_ν, the coupling constant, b_{CN}, was varied freely and the amplitude scaling factor λ was varied within the narrow range of values determined for strong couplings, for which this parameter can be easily determined. The reported uncertainties are at the 95% confidence level according to the following procedure [30]. First, b_{CN} and λ are varied to determine the best-fit dipolar coupling, $\chi^2_{\nu,\mathrm{min}}$. Next, several trial b_{CN} values are selected about the best-fit, and the data are re-fit by optimizing λ within the previously defined range. The uncertainties are represented by χ^2_ν values that differ from $\chi^2_{\nu,\mathrm{min}}$ by $F(\nu)^*\chi^2_{\nu,\mathrm{min}}$ where $F(\nu)$ is a constant that depends on the number of degrees of freedom, ν, and the confidence level. For the case of 95% confidence, and 2 degrees of freedom, $F(\nu) = 19$.

Each best-fit b_{CN} value was linearly scaled by dividing by 0.95 in order to account for thermal motion at 298 K. Internuclear C–N distances are related to the dipolar coupling constants by the equation $b_{CN} = -\frac{\mu_0 \gamma_C \gamma_N \hbar}{4\pi r_{CN}^3}$ [31].

The orientation of the nitrogen in the CSA principle axis system was determined by fitting the experimentally observed REDOR curves (see Fig. 6) of each sideband to numerical simulations explained previously [32]. The weighted χ^2, χ^2_ν, was minimized to fit the data. $\chi^2_\nu \propto \sum_{i,N} w(S_{\exp} - S_{sim})^2$, where the sum is taken over spectral bands *N*, and mixing times *i*. As before, w_i is the inverse uncertainty in each point squared (σ^{-2}). The uncertainties in the dipolar and azimuthal angles alpha and beta are represented by χ^2_ν values that differ from $\chi^2_{\nu,\min}$ by $F(\nu)^* \chi^2_{\nu,\min}$ where $F(\nu)$ is a constant that depends on the number of degrees of freedom, ν, and the confidence level. The best-fit dipolar coupling is used in this determination, so this is really a three-parameter fit. However, since the REDOR dephasing is approximately linear in the beginning of the curve (before the first extremum in the REDOR curve, where we fit the data) a small error in the dipolar coupling does not significantly alter the position of the best-fit orientation, and thus can be treated as a two parameter fit.

Acknowledgments

A.B.B. was supported through an NSF graduate research fellowship. We thank Marvin Bayro for supplying the pulse sequence for the NCCN experiment and Jozef Lewandowski and Matthew Eddy for helpful discussions, and Matthias Zeller for the crystal structure. This research was supported by the National Institutes of Health (EB003151 and EB002026).

References

1. Morcombe CR, Gaponenko V, Byrd RA, Zilm KW. Diluting abundant spins by isotope edited radio frequency field assisted diffusion. J. Am. Chem. Soc. 2004; 126:7196–7197. [PubMed: 15186155]
2. Takegoshi K, Nakamura S, Terao T. C-13–H-1 dipolar-assisted rotational resonance in magic-angle spinning NMR. Chem. Phys. Lett. 2001; 344:631–637.
3. Lewandowski JR, de Paepe G, Griffin RG. Proton assisted insensitive nuclei cross polarization. J. Am. Chem. Soc. 2007; 129:728–729. [PubMed: 17243786]
4. Gullion T, Schaefer J. Rotational-echo double-resonance NMR. J. Magn. Res. 1989; 81:196–200.
5. Bennett AE, Rienstra CM, Griffiths JM, Zhen WG, Lansbury PT, Griffin RG. Homonuclear radio frequency-driven recoupling in rotating solids. J. Chem. Phys. 1998; 108:9463–9479.
6. Gregory DM, Mitchell DJ, Stringer JA, Kiihne S, Shiels JC, Callahan J, Mehta MA, Drobny GP. Windowless dipolar recoupling – the detection of weak dipolar couplings between spin-1/2 nucleic with large chemical-shift anisotropies. Chem. Phys. Lett. 1995; 246:654.
7. Rienstra CM, Tucker-Kellogg L, Jaroniec CP, Hohwy M, Reif B, McMahon MT, Tidor B, Lozano-Perez T, Griffin RG. De novo determination of peptide structure with solid-state magic-angle spinning NMR spectroscopy. Proc. Natl. Acad. Sci. USA. 2002; 99:10260–10265. [PubMed: 12149447]
8. Ramachandran R, Ladizhansky V, Bajaj VS, Griffin RG. ^{13}C–^{13}C rotational resonance width distance measurements in uniformly ^{13}C-labeled peptides. J. Am. Chem. Soc. 2003; 125:15623–15629. [PubMed: 14664610]
9. Costa P, Sun B, Griffin RG. Rotational resonance NMR: separation of dipolar coupling and zero quantum relaxation. J. Magn. Res. 2003; 164:92–103.

10. Andreas LB, Mehta AK, Mehta MA. Determination of global structure from distance and orientation constraints in biological solids using solid-state NMR spectroscopy. J. Am. Chem. Soc. 2007; 129:15233–15239. [PubMed: 17990880]
11. van der Wel PCA, Eddy MT, Ramachandran R, Griffin RG. Targed ^{13}C-^{13}C distance measurements in a microcrystalline protein via J-decoupled rotational resonance width measurements. Phys. Chem. Chem. Phys. 2009; 10 in press.
12. Ramachandran R, Lewandowski JR, van der Wel PCA, Griffin RG. Multipole-multimode Floquet Theory of rotational resonance width experiments: ^{13}C–^{13}C distance measurements in uniformly labeled solids. J. Chem. Phys. 2006; 124:214107. [PubMed: 16774398]
13. Costa PR, Gross JD, Hong M, Griffin RG. Solid-state NMR measurement of Psi in peptides: a NCCN 2Q-heteronuclear local field experiment. Chem. Phys. Lett. 1997; 280:95–103.
14. Wu S, Declercq JP, Tinant B, Vanmeerssche M. Crystal-structure and conformation of short linear peptides.6. l-Alanyl-l-prolyl-glycine monohydrate. Bull. Soc. Chim. Belg. 1987; 96:515–520.
15. Levitt MH, Raleigh DP, Creuzet F, Griffin RG. Theory and simulations of homonuclear spin pair systems in rotating solids. J. Chem. Phys. 1990; 92:6347–6364.
16. Ramachandran R, Griffin R. Multipole-multimode Floquet Theory in nuclear magnetic resonance. J. Chem. Phys. 2005; 122:164502. [PubMed: 15945688]
17. Bak M, Schultz R, Vosegaard T, Nielsen NC. Specification and visualization of anisotropic interaction tensors in polypeptides and numerical simulations in biological solid-state NMR. J. Magn. Res. 2002; 154:28–45.
18. Herzfeld J, Berger AE. Sideband intensities in NMR spectra of samples spinning at the magic angle. J. Chem. Phys. 1980; 73:6021–6030.
19. Ye C, Fu R, Hu J, Hou L, Ding S. Carbon-13 chemical shift anisotropies of solid amino acids. Magn. Reson. Chem. 1993; 31:699–704.
20. Bayro MJ, Huber M, Ramachandran R, Davenport TC, Meier BH, Ernst M, Griffin RG. Dipolar truncation in magic-angle spinning NMR recoupling experiments. J. Chem. Phys. 2009; 130:114506. [PubMed: 19317544]
21. Brunger AT, Adams PD, Clore GM, DeLano WL, Gros P, Grosse- Kunstleve RW, Jiang JS, Kuszewski J, Nilges M, Pannu NS, Read RJ, Rice LM, Simonson T, Warren GL. Crystallography & NMR system: a new software suite for macromolecular structure determination. Acta Crystallogr. D Biol. Crystallogr. 1998; 54:905–921. [PubMed: 9757107]
22. Brunger AT. Version 1.2 of the crystallography and NMR system. Nat. Protoc. 2007; 2:2728–2733. [PubMed: 18007608]
23. Yaffe MB, Schutkowski M, Shen M, Zhou XZ, Stukenberg PT, Rahfeld J-U, Xu J, Kuang J, Kirschner MW, Fischer G, Cantley LC, Lu KP. Sequence-specific and phosphorylation-dependent proline isomerization: a potential mitotic regulatory mechanism. Science. 1997; 278:1957–1960. [PubMed: 9395400]
24. Hohwy M, Rienstra CM, Jaroniec CP, Griffin RG. Fivefold symmetric homonuclear dipolar recoupling in rotating solids: application to double quantum spectroscopy. J. Chem. Phys. 1999; 110:7983–7992.
25. Bennett AE, Rienstra CM, Auger M, Lakshmi KV, Griffin RG. Heteronuclear decoupling in rotating solids. J. Chem. Phys. 1995; 103:6951.
26. Delaglio F, Grzesiek S, Vuister GW, Zhu G, Pfeifer J, Bax A. NMRpipe – a multidimensional spectral processing system based on unix pipes. J. Biomol. NMR. 1995; 6:277–293. [PubMed: 8520220]
27. Veshtort M, Griffin RG. SPINEVOLUTION: a powerful tool for simulations of solid and liquid state NMR experiments. J. Magn. Res. 2006; 178:248–282.
28. Kaustov L, Kababya S, Belakhov V, Baasov T, Shoham Y, Schmidt A. Inhibition mode of a bisubstrate inhibitor of KDO8P synthase: a frequency-selective REDOR solid-state and solution NMR characterization. J. Am. Chem. Soc. 2003; 125:4662–4669. [PubMed: 12683839]
29. Klug CA, Zhu W, Tasaki K, Schaefer J. Orientational order of locally parallel chain segments in glassy polycarbonate from ^{13}C–^{13}C dipolar couplings. Macromolecules. 1997; 30:1734–1740.
30. Shoemaker D, Garland C, Steinfeld J, Nibler J. Least-Squares fitting procedures. Experiments in Physical Chemistry. 1989

31. Jaroniec CP, Tounge BA, Herzfeld J, Griffin RG. Frequency selective heteronuclear dipolar recoupling in rotating solids: accurate C-13–N-15 distance measurements in uniformly C-13, N-15-labeled peptides. J. Am. Chem. Soc. 2001; 123:3507–3519. [PubMed: 11472123]

32. O'connor RD, Schaefer J. Relative CSA-dipolar orientation from REDOR sidebands. J. Magn. Res. 2002; 154:46–52.

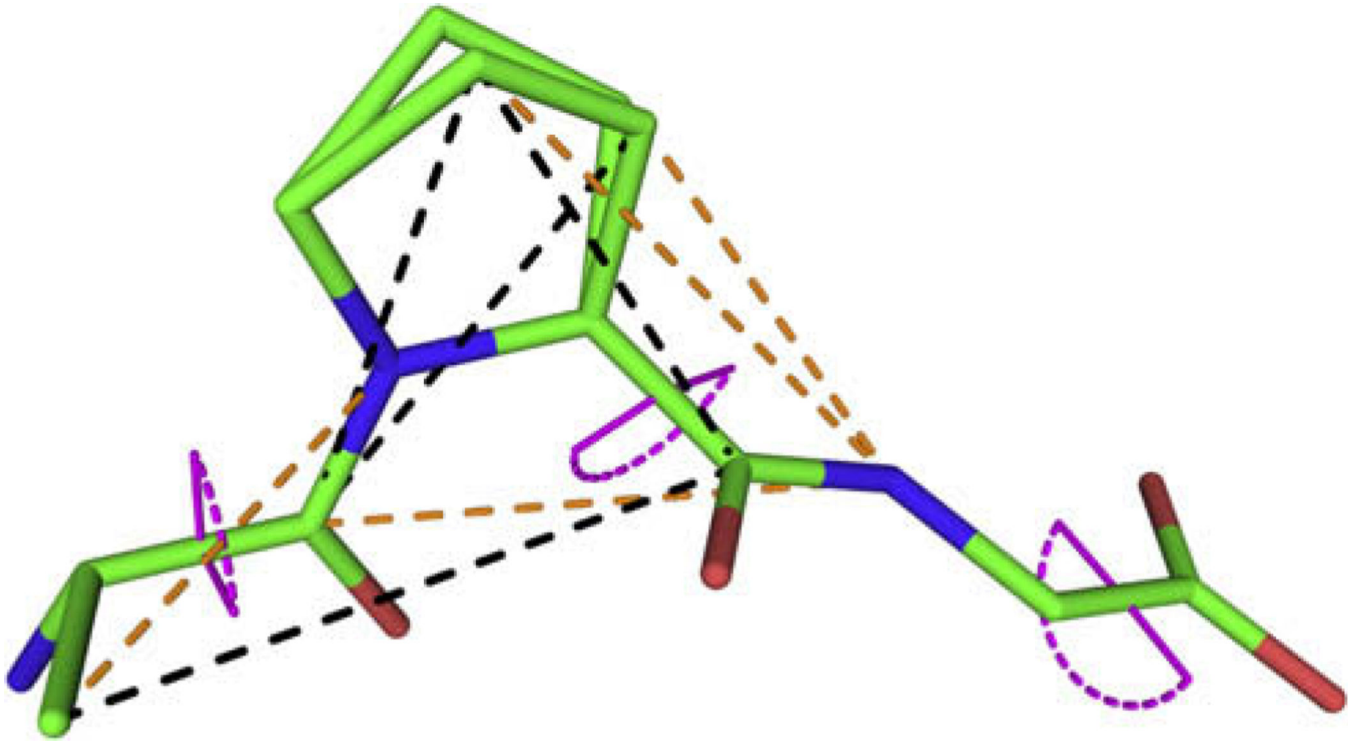

Fig. 1.

Crystal structure of APG [14] showing the 11 SSNMR experimental constraints used in the structural refinement. Torsion angles are displayed in violet, REDOR distances in orange and R^2W constraints in black. Note that the proline ring has a split occupancy between two conformers in the crystal structure. (For interpretation of colour mentioned in this figure, the reader is referred to the web version of this article.)

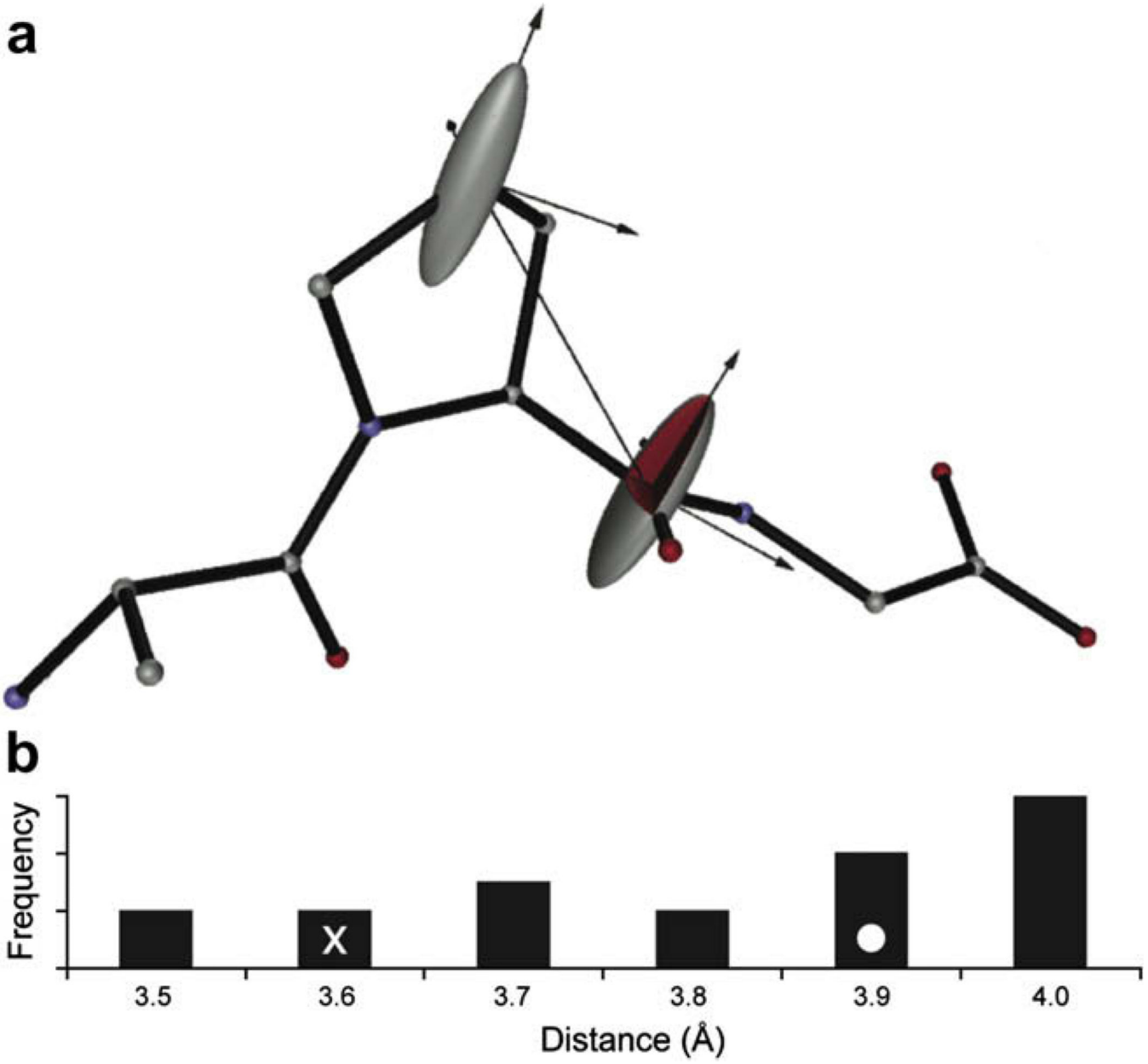

Fig. 2.

(a) Relative orientations of the Proline C′ and Cγ CSAs are shown superimposed on the initial structure calculated using REDOR and torsion angle constraints. (b) Histogram displaying the range of Pro C′-Pro Cγ distances calculated from an ensemble of accessible structures generated using simulated annealing (CNS) without any constraints. X-ray (x) and reported NMR (o) distances are indicated. This graphic was produced with SIMMOL [17].

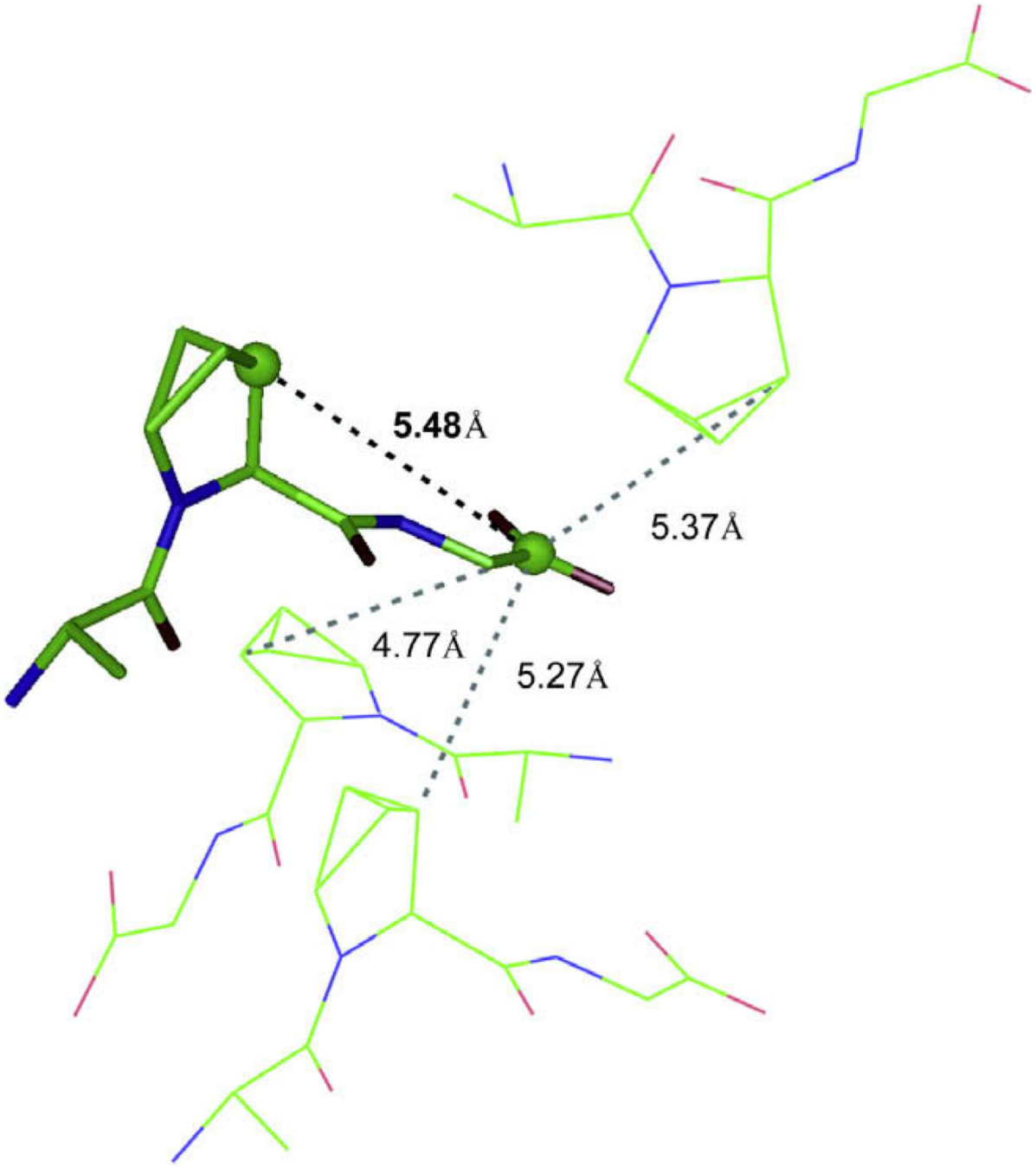

Fig. 3.

Crystal lattice of APG showing competing intermolecular distances to the long-range internuclear distance that could be used for structural refinement.

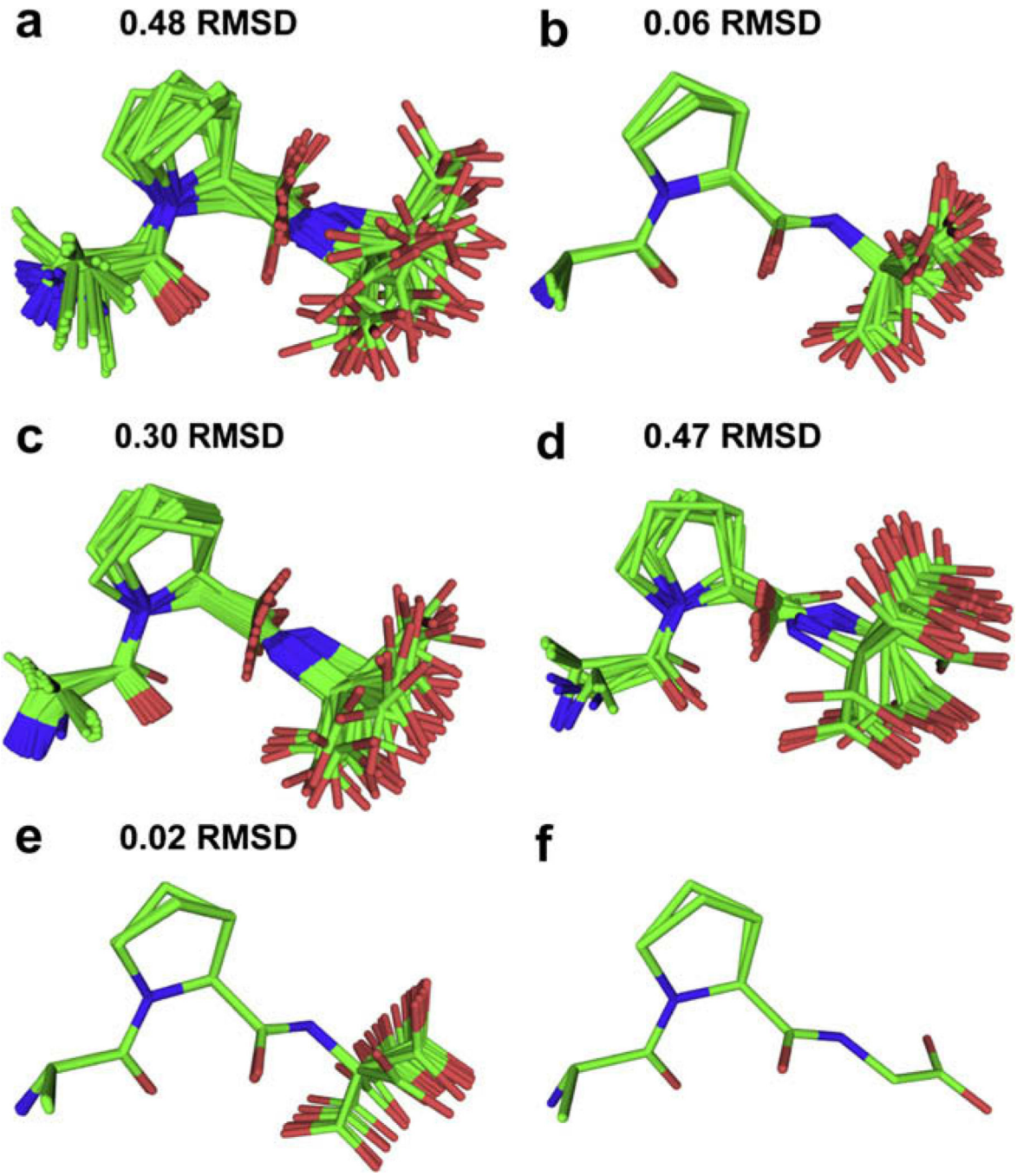

Fig. 4.

Twenty lowest energy structures of APG using simulated annealing (CNS) (a) no constraints (b) 2 ψ angles from NCCN measurements (c) 4 ^{13}C–^{13}C distance constraints (d) 4 ^{13}C–^{15}N heteronuclear constraints (e) all 11 constraints (f) crystal structure.

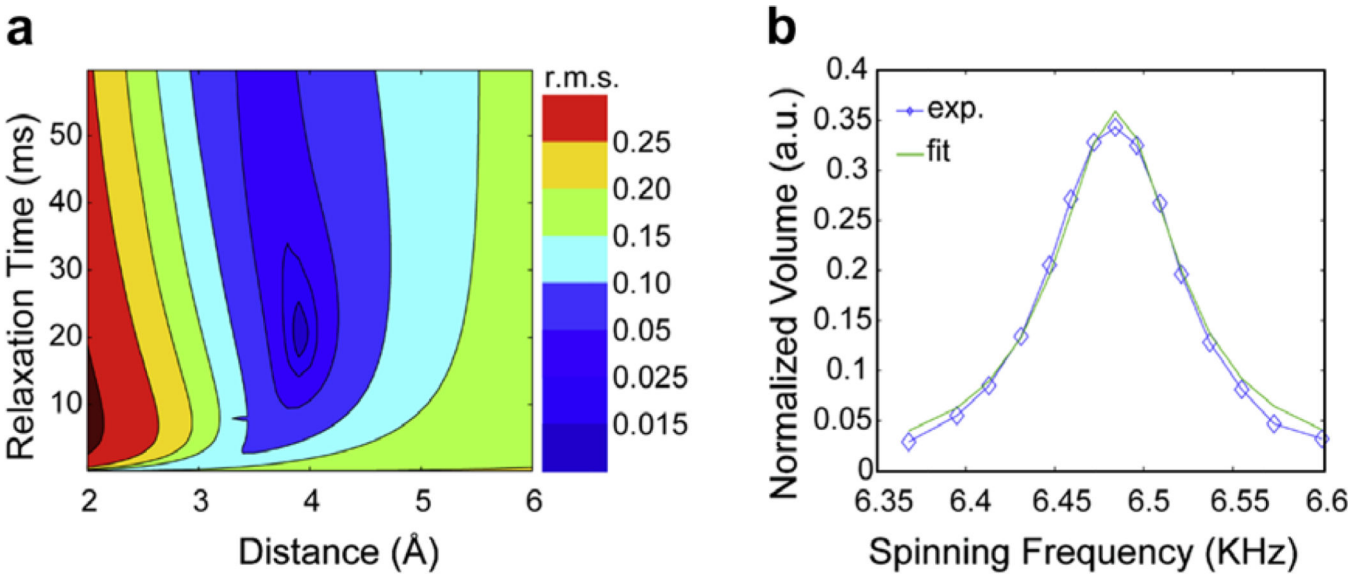

Fig. 5.

(a) Contour plot of the root mean square deviation between experimental and simulated R^2W profiles for P_O to P_γ as a function of distance and relaxation. (b) Magnetization transfer from P_o to P_γ in R^2W as a function of spinning frequency. The experimental data is shown in blue, and the fit in green. (For interpretation of colour mentioned in this figure, the reader is referred to the web version of this article.)

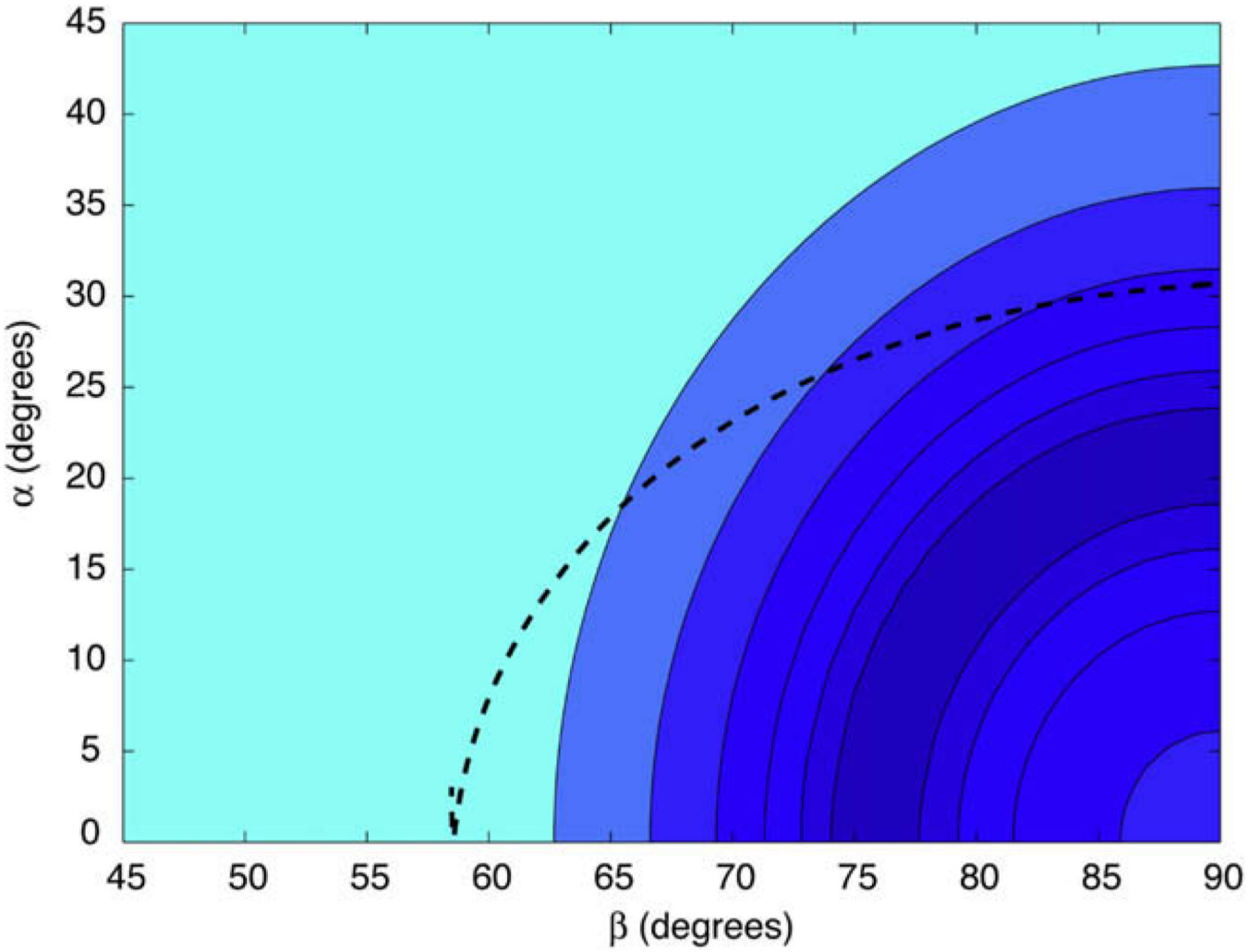

Fig. 6.

The χ^2 surface for azimuthal (α) and polar (β) angles of the CSA-dipole orientation with each contour level two times the previous level. Labeled APG was diluted to 10% in natural abundance APG and data were collected at 14.1 Tesla with an MAS spinning frequency of 8929 Hz. The superimposed dashed line shows the allowed azimuthal and polar angles corresponding to a rotation about the terminal ψ dihedral angle, with the best-fit at $\alpha = 31°$, $\beta = 90°$.

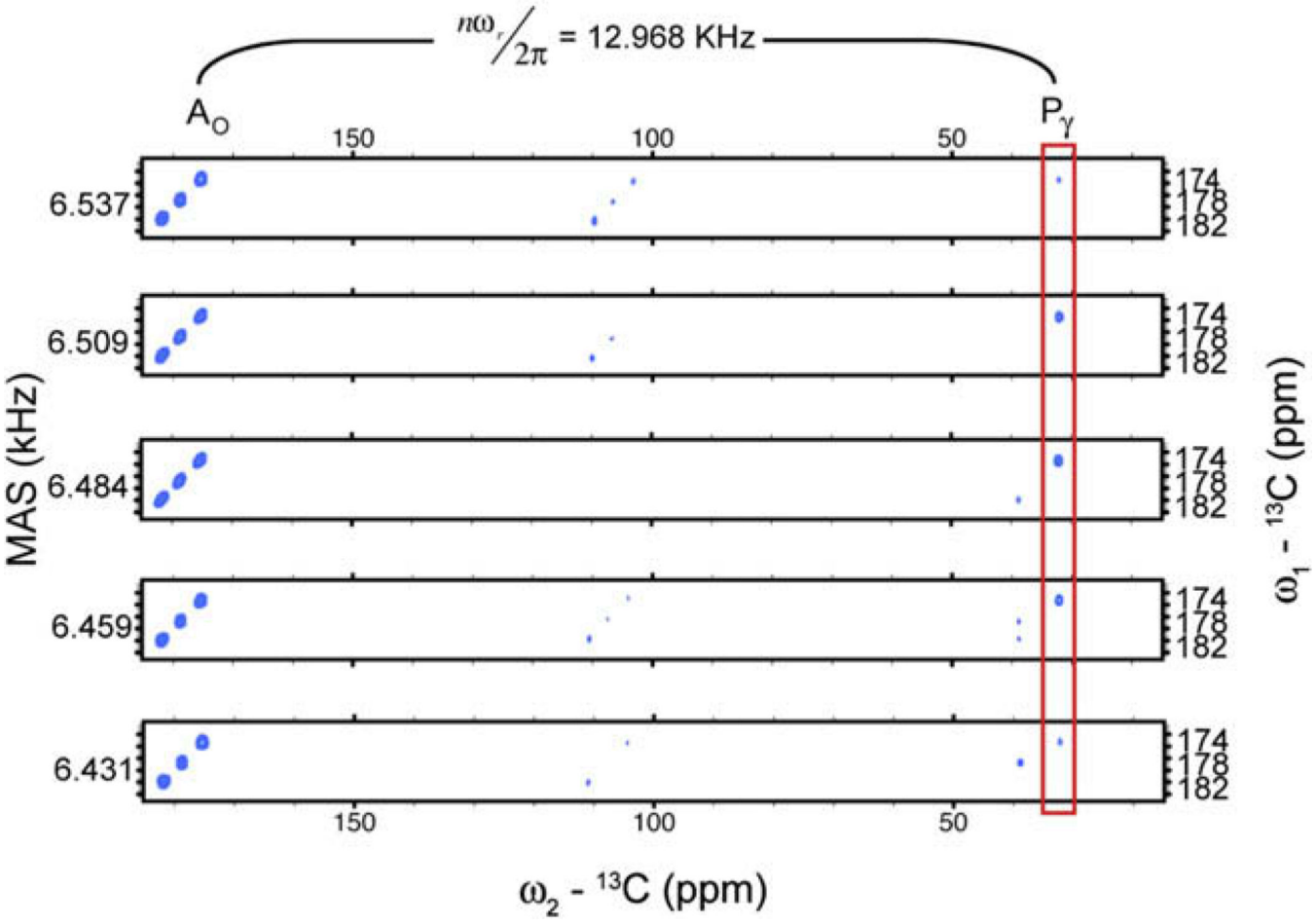

Fig. 7.

R^2W spectra at five spinning frequencies. The P_γ crosspeak intensifies as the spinning frequency is swept the R^2 condition between the spin pair.

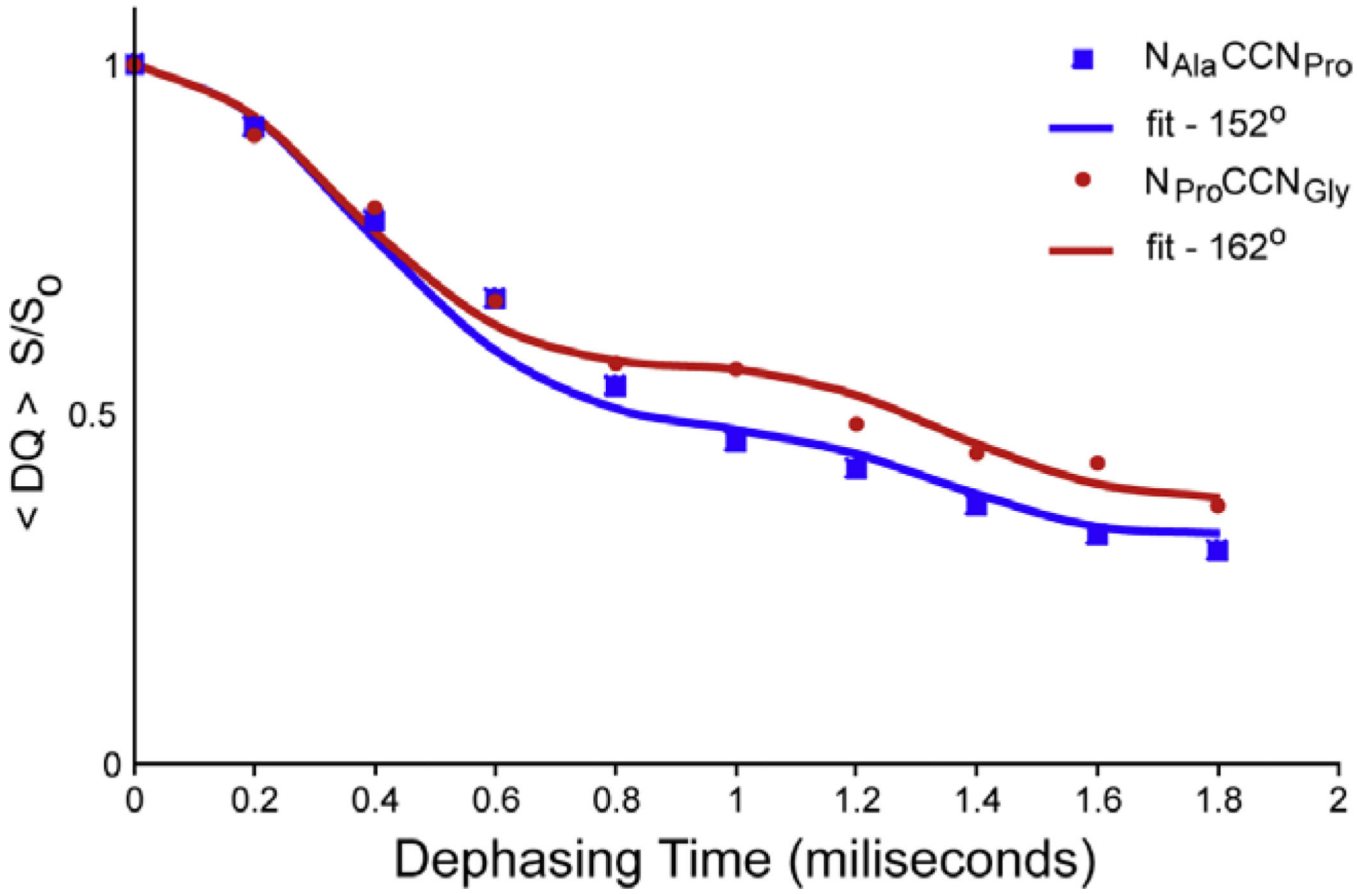

Fig. 8.

Dephasing curves for extraction of Ψ torsion angle. An $N_{Gly}CCN_{Pro}$ Ψ angle of 152° (blue) was extracted compared to 153° from the X-ray data and $N_{Ala}CCN_{Gly}$ Y angle was found to be 162° (red) versus 157° from the X-ray data. SPINEVOLUTION [27] was used to fit the data. (For interpretation of colour mentioned in this figure, the reader is referred to the web version of this article.)

Table 1

Experimental solid-state NMR constraints used in the structure calculation and corresponding values from the crystal structure from all NMR experiments; DANTE-REDOR (orange), NCCN torsion angles and R^2W distances (black).

ψ Torsion Angles	**X-ray (°)**	**SSNMR (°)**
ψ_{Gly}	178	180 ± 15
ψ_{Ala}	153	152 ± 5
ψ_{Pro}	157	162 ± 5
Distances	X-ray (Å)	SSNMR (Å)
Pro N–Ala C^{β}	3.2	3.2 ± 0.1
Gly N–Pro C^{β}	3.2	3.2 ± 0.15
Pro C′–Pro C^{γ}	3.3/3.6	3.9 ± 0.39
Ala C′–Pro C^{β}	3.6	3.8 ± 0.38
Ala C′–Pro C^{γ}	3.6	3.9 ± 0.39
Gly N–Ala C′	4.1	4.1 +0.6/−0.3
Gly N–Pro C^{γ}	4.5/4.3	4.2 +0.6/−0.3
Pro C′–Ala C^{β}	4.7	4.4 ± 0.44